INSTRUMENTATION

Characteristics of a Scanning, Multidetector, Single-Photon ECT Body Imager

Carl-Martin Kirsch, Stephen C. Moore, Robert E. Zimmerman, Robert J. English, and B. Leonard Holman

Harvard Medical School and Brigham and Women's Hospital, Boston, Massachusetts

We evaluated a single-photon emission computed tomographic system using ten scanning detectors in a circular array. The system uses focusing collimators that scan radially as well as tangentially.

The spatial resolution in the tomographic plane is 2.6 cm FWHM and the axial resolution is 3.3 cm FWHM. The resolution is independent of position within the field of view, and nearly independent of energy through 511 keV. Sensitivity was found to be 4600 cps/μCi-ml for an extended phantom, 20-cm in diameter, filled with Tc-99m; 7200 cps/μCi-ml with Tl-201; and 8000 cps/μCi-ml with Ga-67. Investigations of positional uniformity indicated some quantitative distortion of data due to inadequate attenuation correction. Improvement in the attenuation correction is necessary before truly quantitative tracer distribution studies are undertaken.

J Nucl Med 22: 726–731, 1981

Several single-photon tomography techniques are now being investigated to improve quantitative capabilities in nuclear medicine. Longitudinal tomography with gamma cameras can be performed by coded apertures (*1*) or by collimators with several pinholes (*2*). In general these methods lack quantitative capabilities, sensitivity, and uniformity of spatial response (*3*). A conventional gamma camera, rotating around the patient, can be used for quantitative transaxial tomography, but here again the spatial response varies within the transverse slice (*4,5*).

For single transverse tomographic sections, the use of multiple scanning detectors placed around the patient has theoretical advantages over these other types of systems, such as higher sensitivity and more uniform spatial resolution (*6,7*). We have determined the physical characteristics of such an instrument designed for body imaging and modified by us for physical and clinical imaging evaluations.

Received Oct. 27, 1980; revision accepted March 26, 1981.

For reprints contact: B. Leonard Holman, MD, Dept. of Radiology, Harvard Medical School, 25 Shattuck St., Boston, MA 02115.

METHODS

Scanner operation. This instrument obtains transaxial emission tomograms using a circular configuration of ten NaI(Tl) detectors 20 cm × 12.5 cm × 2.5 cm (Fig. 1), equipped with focused collimators. The physical properties of the collimators are listed in Table 1. Each detector scans the circular field of view, 51 cm in diameter, tangentially with its focal point moving through the object. After a line is scanned, one detector is moved radially outward while its opposing detector is moved inward the same distance. The next tangential line is then scanned. Each of the ten detectors scans half the total field of view. The entire ring of detectors is then rotated

TABLE 1. LINE-SOURCE RESPONSE OF THE COLLIMATOR AT THE FOCAL POINT*

	Tangential	Axial	Radial
FWHM (cm)	1.6	2.0	24.0
FWTM (cm)	2.4	3.0	—

* Focal length = 42 cm.

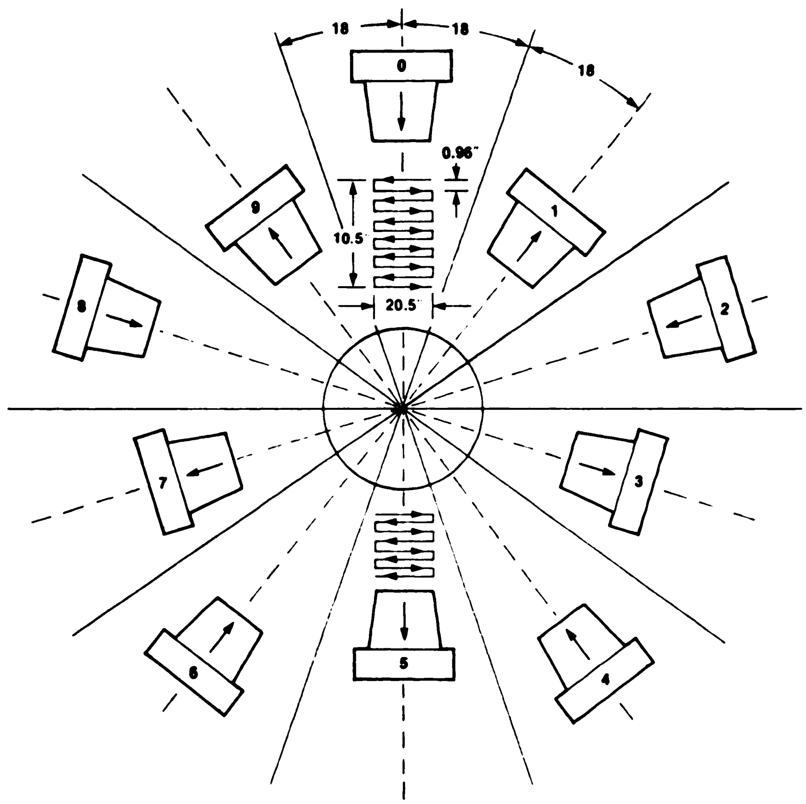

FIG. 1. Detector arrangement and scan pattern for whole-body imager.

18° (half the angular separation between detectors) and the same scan pattern is repeated, resulting in 20 projections, at 18° intervals, for the reconstruction of one transverse slice. The scan time is 5 min per slice.

The system can perform dual-nuclide or dual-energy studies, since there are two independent data channels, each with its own adjustable pulse-height window.

The unusual scan pattern and the use of point-focusing collimators leads to a reconstruction procedure somewhat different from that associated with tomographic machines having parallel holes, pinholes, or converging collimators. First, each data projection is corrected for attenuation using a simple, uniform exponential correction. Before the scan starts, the operator enters the radius of the object being scanned. The correction grid calculation assumes a circular object of uniform density, centered within the gantry. This is a first-order approximation to an attenuation correction, since it does not account for variable attenuation or nonuniform source distributions within the attenuation material.

Each row of data is then filtered using a one-dimensional convolution filter. The filter has a medium-pass (ramp with roll off) response that has been empirically determined by iteratively varying the coefficients to produce the optimal reconstruction of a cylindrical phantom with three separate concentric regions of different activity concentrations. The inner circle and the outermost annulus had the same concentrations and the middle annulus had no radioactivity. The convolving filter is somewhat different from that used for rotating gamma-camera systems with parallel-hole collimators because of the different scan geometry and collimation (*7*).

Each convolved data point is interpolated onto the 128 × 128 reconstruction grid at its focal-point position. This is because the instrument uses focused collimators and the detectors move in and out radially in addition to scanning tangentially. This produces uniform spatial resolution and sensitivity over the whole field of view.

Measurements. For most of the experiments we used a standard ECT performance phantom* with a 20-cm diameter and a 35-cm length. A special fixture was designed for mounting plastic vials (2.5 × 5.0 cm) within the phantom, allowing various geometric configurations. The latest version of the software was used for all data acquisition and reconstruction.

Pulse-height analyzer energy window. The window setting of the analyzer must be optimized for good counting rate and image contrast. If the lower limit of the energy window is too low, many scattered photons appear in the image, thus degrading contrast. On the other hand, too narrow a window decreases the number of recorded counts. Poor statistics also leads to a low signal-to-noise ratio. A phantom experiment was performed using a radioactive flood source containing two water-filled, zero-activity vials, one on center and the other 5 cm off center. The isotope concentration was 1.5 μCi/cc, giving a count rate high enough for narrow window settings. The experiment was run for three different nuclides: Tc-99m, Tl-201, and Ga-67. A pulse-

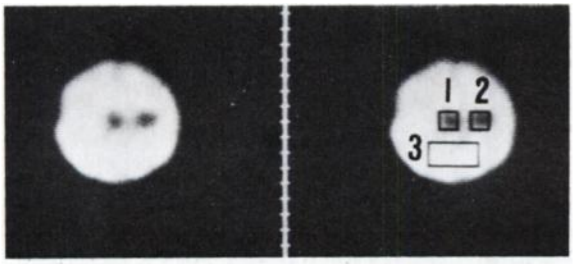

FIG. 2. Flood source (20 cm diam) with regions without activity centered and 5 cm off center (left). Regions of interest used to determine image contrast (1,2,3) and noise (3) (right).

height spectrum of each was obtained, and the upper limit was set to 170 keV (5% of peak count) for Tc-99m, and 90 keV (20% of peak count) for Tl-201. For Ga-67, each photopeak was treated differently. Due to overlap and scatter, a clear separation between the individual peaks was not possible. Consequently the upper limit for each peak was set to the peak energy plus 20 keV. For each emitter, scans were performed for several different values of the lower energy window setting. For each setting we evaluated image contrast (see Fig. 2) first calculating a modulation index M_i for each of the two zero-activity regions.

$$M_i = \frac{\bar{x} - \min_i}{\bar{x} + \min_i} \quad (i = 1,2),$$

where $\bar{x}$ is the average pixel count in a region of interest where uniform activity distribution was present (Region 3), and $\min_i$ is the average of the four minimum pixels in Region i. To include the effects of image noise in the contrast evaluation, we further define a figure of merit as FOM = $(M_1 + M_2)/2\sigma$, where σ is the root-mean-square deviation in Region 3. The window setting for maximum FOM was used for all further experiments. Subsequent measurements with Ga-67 used only the two lower energy peaks, summed in dual-peak mode.

Sensitivity. The standard phantom was used to determine both counting-rate sensitivity and regional sensitivity for Tc-99m, Tl-201, and Ga-67. The counting sensitivity for a 20-cm flood phantom was the number of total counts recorded per second per unit concentration of the radionuclide. The regional sensitivity was defined as the average number of counts per resolution element per unit concentration in two regions of interest (2.6 cm × 2.6 cm), one in the center, one near the edge. For the regional sensitivity measurements, the attenuation corrections were made with the phantom centered in the field of view.

Linearity. For this measurement, a 585-ml annular phantom (i.d. 88 mm, o.d. 113 mm) was filled with a solution of Tc-99m. The concentration was increased several times and the total number of counts recorded for each concentration. The annular phantom was used instead of a circular flood to obtain a high radionuclide concentration with a lower total dose.

Line-spread functions. To measure the resolution of the machine when imaging activity inside a scattering medium, a "line" source (1.5 mm diam) was inserted in the center of the 20-cm phantom, which was filled with water. The resolution within the scanned slice was evaluated for all three radionuclides by measuring the full width at half maximum (FWHM) and full width at tenth maximum (FWTM) of the line-spread functions. The response in the axial (interslice) direction was measured by scanning the line source inserted in the center of the phantom at an angle of 45° to the cylindrical z axis.

To study the positional dependence of the resolution within a slice, a Tc-99m scan was recorded with the line source placed 7.5 cm from the center of the phantom. The phantom with the off-center line source was then rotated 9° (half the angular spacing between projections) and a final scan was obtained to test for possible systematic differences due to the limited number of projections.

Noise. For an ideal tomographic machine, we would expect the image noise (expressed as % standard deviation) to be inversely proportional to the square root of the average pixel count. In addition the reconstruction process amplifies the Poisson noise associated with detecting radioactively decaying nuclides. To test the noise properties of this machine, the 20-cm flood phantom was filled with a concentration of 1.4 μCi/cc of Tc-99m, and scanned periodically for four half-lives. The percentage standard deviation inside a region of interest was then calculated as a function of total counts.

Positional uniformity. To measure the positional uniformity of the machine for a simple distribution of radionuclide concentration a 35-cm phantom was filled with Tc-99m at a concentration of 0.5 μCi/cc. A moveable cylindrical vial, 5 cm in diameter, was filled with a concentration of 5.5 μCi/cc and placed inside the larger flood. Three scans were made with the vial centered, 9 cm off-center, and 14 cm off-center. The average pixel count in regions inside and outside the activity was recorded.

Imaging higher-energy photons. To image single 511-keV photons from positron annihilation events, we reduced the photomultiplier tube gain until the signal amplitude for a given emitter was half its value for normal machine operation. This was necessary because the

TABLE 2. ENERGY RESOLUTION

Energy (keV)	Resolution (%)
70 (Tl-201)	34
140 (Tc-99m)	22
280 (Hg-201)	18
511 (Ga-68)	14

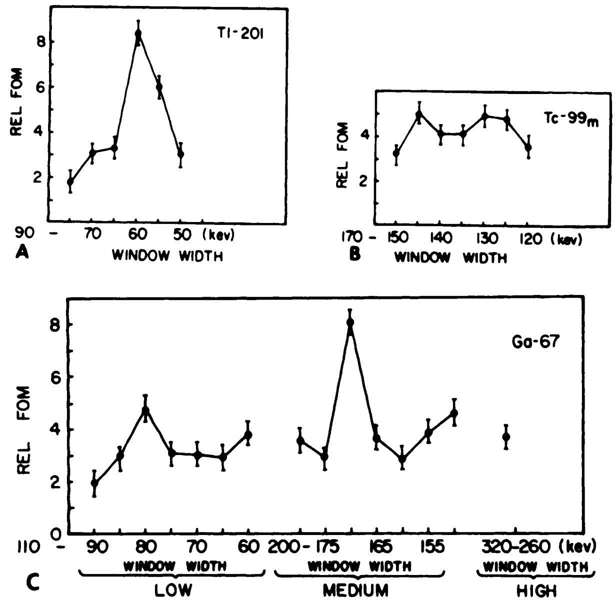

FIG. 3. Figure of merit used to determine the pulse-height window for Tl-201 (A), Tc-99m (B), and Ga-67 (C).

pulse-height analyzer preamplifier circuits do not respond properly to such large signals.

For this reduced-gain mode of operation the energy resolution of the 280-keV photopeak of Hg-203 was ~18%. The energy resolution of the 511-keV annihilation photons from Ga-68 was ~14%. For all scans, we set the PHA window asymmetrically around the photopeak, just as with the other emitters. We first measured the intraslice and interslice resolution by scanning a Ga-68 line source in air.

To study the effects of shielding "punch-through" by high-energy photons originating outside the scanned slice, we placed a second, larger source (150 ml) containing roughly three times the activity of the line source, 20 cm outside the scan field in the z direction and 25 cm off-center to the right (x direction). We then scanned the line source fixed in the center of the scan field.

RESULTS

The percent energy resolution was measured for several emitters over a wide range of energies. The results are shown in Table 2.

The figure-of-merit plots for optimizing the PHA window settings are shown in Fig. 3. The windows chosen for all other experiments were 60–90 keV for Tl-201; 130–170 keV for Tc-99m; 80–110 keV for the low-energy peak of Ga-67; and 170–200 keV for its medium-energy peak. The high energy peak of Ga-67 was not evaluated because of its small contribution to the overall spectrum.

The total count sensitivity and regional sensitivity are listed in Table 3.

Figure 4 shows the linearity measurement, which is

TABLE 3. SENSITIVITY

	20-cm flood source ($cps/\mu Ci$-ml)	Regional (5 min scan time)
Tc-99m	4,600	29,800*
Tl-201	7,200	48,100
Ga-67	8,000	52,300

* Counts/μCi-ml, per resolution element (2.6 × 2.6 cm).

plotted as total counting rate against Tc-99m concentration. It is seen that the counting rate is linear up to ~5 μCi/cc in the annular phantom.

The FWHM and FWTM of the line-spread functions for all four emitters are listed in Table 4. The larger values of FWTM for the low-energy nuclides are due to a greater number of scattered photons present in the image. The high values for Ga-68 are the result of 511-keV photons "punching-through" the lead collimators. The Tc-99m line-spread function was the same when the source was moved 7.5 cm off-center, both in the horizontal direction and rotated. In Fig. 5 the image noise is plotted against total counts, expressed as percent standard deviation (% rms deviation) in a region of interest. The curve was produced by fitting the data to the function

$$\% \text{ rms} = \frac{a}{\sqrt{N_{tot}}},$$

where a is the parameter determined by the fit.

The uniformity for imaging a high-activity vial inside a uniform flood phantom (concentration ratio 10.8:1) varied considerably with position of the source. In the center the measured ratio was 5.6; 9 cm off-center, 11.1; and 14 cm off-center 13.0.

Figure 6 shows the reconstruction of a line source of Ga-68. As previously described, this source was scanned

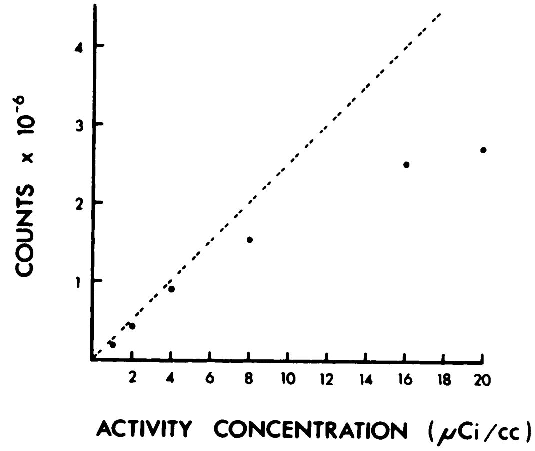

FIG. 4. Linearity of imaging device.

TABLE 4. SPATIAL RESOLUTION

	Intraslice		Interslice	
	FWHM (cm)	FWTM (cm)	FWHM (cm)	FWTM (cm)
Tl-201	2.8 ± 0.2	6.0 ± 0.2	3.8 ± 0.2	7.2 ± 0.2
Tc-99m	2.6 ± 0.2	4.5 ± 0.2	3.3 ± 0.2	5.3 ± 0.2
Ga-67	2.8 ± 0.2	6.2 ± 0.2	3.5 ± 0.2	5.9 ± 0.2
Ga-68*	3.0 ± 0.2	8.4 ± 0.2	5.2 ± 0.2	—

* Line source in air.

in the presence of a larger source *outside* the field of view, with approximately three times the line-source activity. The effects of 511-keV photons "punching through" the detector shielding and collimators can be seen clearly in the image. The source outside the scan plane was placed in what we believe to be a "worst-case" position.

DISCUSSION

Multidetector imaging systems for transaxial computed tomography have properties that could lead to the accurate measurement of radionuclide distribution concentrations (*6–12*). We find that this type of imager has good sensitivity for a wide range of photon energies. The instrument also has good linearity up to ~5 μCi/cc, and dose concentrations for most nuclear medicine procedures seldom exceed this value. In contrast to rotating gamma camera systems, the spatial resolution of this scanner is constant throughout the scanned slice. Using a rotating gamma camera with 20-cm radius of rotation and a high-resolution collimator, Jaszczak et al. (*5*) determined the resolution of a line source in various positions inside an elliptical phantom (30.5 × 22.5 cm) filled with water. The measured FWHM of the line-spread function varied from 16 mm in the center to 14 mm when the source was placed 12 cm off center. Even greater variation would be expected if (a) a clinically more suitable collimator had been used, (b) the measurements had been continued up to the edge of the field of view, or (c) data had been acquired over 180° only.

The image noise as a function of total counts for a 20-cm flood phantom of Tc-99m (4 mm × 4 mm pixels) is given by

$$\%\ \text{rms} = \frac{6800}{\sqrt{N_{tot}}}.$$

We have compared the properties of this multidetector scanner with the published results obtained from a single-head, 25-cm-diameter rotating gamma camera system with the same spatial resolution. From an analysis by Budinger et al. (*13*), we calculate that such a camera system (with pixels 1.5 times the size of the projection bins, and 144 angular projections) would amplify the Poisson noise by ~2140. The noise amplification (×3.2) for the scanning multidetector system, however, is somewhat mitigated by its high (single-slice) sensitivity. In fact, this system could have a single-slice counting rate about seven times that of the rotating camera system if its scan were restricted to half the field of view (radially and tangentially).

Huesman (*14*) has studied the theoretical dependence of image noise on the angular and lateral sampling frequencies. From this analysis, we calculate that the image noise of a rotating gamma camera system would increase by a factor of 4.0 if only 10 projections were recorded in 180° instead of 144. Since the noise amplification of the scanning multidetector system is 3.2 times that of a camera recording 144 projections, it seems that the limited number of angular projections is compensated somewhat by scanning in and out radially with focused collimators in addition to the tangential scanning. Nevertheless, the recording of more angular projections in the same scan time would substantially de-

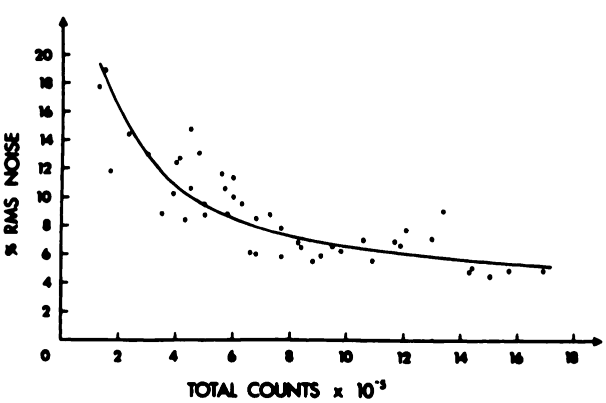

FIG. 5. Percent root-mean-square (% rms) noise as a function of average pixel count in a large region of interest. Curve shown results from least-squares fit to the form: % rms noise = $a/\sqrt{N_{tot}}$. Parameter determined by fit is a = 6,800. Standard deviation of data points with respect to fitted function is 1.78%.

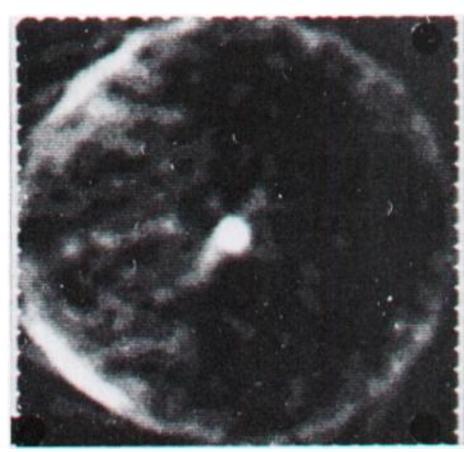

FIG. 6. Effects of shield penetration by 511-keV photons. Line source filled with Ga-68 in center of field of view with a large source outside and to the left of scan plane.

crease the noise amplification while maintaining the high sensitivity.

At present, the major drawback to this system is its poor resolution and positional dependence of quantitative measurements. Given the intrinsic physical properties of the instrument, it is likely that an overly simplistic attenuation correction is responsible for the position dependence of the concentration-ratio measurements. We are currently working on a different method of attenuation correction, which should greatly improve the machine's quantitative capabilities.

Most of the physical measurements are highly dependent on the version of the software used. Using software revision 1.1, Jarritt and Ell (*11*) reported measurements of spatial resolution and detector sensitivity for Tc-99m that differ significantly from our results using revision 2.1. Revision 1.1 contained program errors that caused a higher number of total counts to be reported than were actually detected. This may explain their higher sensitivity measurement. Revision 1.1 also used a convolution filter with a higher frequency cutoff, which produced lower values for spatial resolution. However, this filter was modified in a subsequent version (as previously discussed) to reduce artifacts and improve uniformity. Our measurements are based on this improved filter.

We found that the system has a considerably higher sensitivity for Tl-201 and Ga-67 than for Tc-99m. This is due to the presence of more scattered photons with energies inside the pulse-height windows for the former two. However, these photons must have scattered through relatively small angles, since the contrast ratio (figure of merit) was higher than for Tc-99m. Thus it seems that the high sensitivity is solely responsible for the higher contrast ratio in images with Tl-201 and Ga-67.

This instrument is not expected to image positron-emitting radionuclides as accurately as coincidence tomography systems (*15*). Nevertheless, it is interesting to observe that even with a "worst case" background source outside the scanned section, this machine is capable of obtaining acceptable images with such high-energy photons, and this would be useful for dual-nuclide studies using, for example, Rb-81 and Kr-81m for measurements of regional blood flow.

FOOTNOTE

* Nuclear Associates.

ACKNOWLEDGMENTS

We received help for this work from several scientists and engineers. We particularly wish to acknowledge Nicholas Accomando, Jacques Brunelle, and Robert Manna.

We also thank Margaret J. R. Senechal and Janice Neumann for their expert secretarial assistance.

This work was supported in part by a grant from the USPHS HL-26215 and by a NATO Fellowship provided by the German Academic Exchange Service.

REFERENCES

1. ROGERS WL, KORAL KF, MAYANS R, et al: Coded-aperture imaging of the heart. *J Nucl Med* 21:371-378, 1980
2. VOGEL RA, KIRCH D, LEFREE M, et al: A new method of multiplanar emission tomography using a seven pinhole collimator and an Anger scintillation camera. *J Nucl Med* 19: 648-654, 1978
3. WILLIAMS DL, RITCHIE JL, HARP GD, et al: In vivo simulation of thallium-201 myocardial scintigraphy by seven-pinhole emission tomography. *J Nucl Med* 21:821-828, 1980
4. BUDINGER TF, DERENZO SE, GULLBERG GT, et al: Emission computer assisted tomography with single-photon and positron annihilation photon emitters. *J Comput Assist Tomogr* 1:131-145, 1977
5. JASZCZAK RJ, CHANG L-T, STEIN NA, et al: Whole-body single-photon emission computed tomography using dual, large-field-of-view scintillation cameras. *Phys Med Biol* 24: 1123-1143, 1979
6. ZIMMERMAN RE, KIRSCH C-M, LOVETT RD, et al: Single photon emission computed tomography with short focal length detectors. In *Single Photon Emission Computed Tomography and Other Selected Computer Topics.* Price RR, Gilday DL, Croft BY, Eds. New York, Society of Nuclear Medicine, 1980, pp 147-157
7. STODDART HF, STODDART, HA: A new development in single gamma transaxial tomography: Union Carbide focussed collimator scanner. *IEEE Trans Nucl Sci* NS-26:2710-2712, 1979
8. HOLMAN BL, HILL TC, LOVETT RD, et al: Double-tracer, multiple-organ transaxial emission computed tomography: Improved localization and characterization of radiotracer distributions. *Radiology* 135:435-438, 1980
9. HOLMAN BL, HILL TC, WYNNE J: Single-photon transaxial emission computed tomography of the heart in normal subjects and in patients with infarction. *J Nucl Med* 20: 736-740, 1979
10. HILL TC, ZIMMERMAN RE: Single-photon ECT of the brain: System performance and clinical utility. Proceedings of Bureau of Radiological Health Conference on Computed Tomography. Washington, DC, 1980, in press
11. JARRITT PH, ELL PJ: A new emission tomographic body scanner. *Nucl Med Commun* 1:94-101, 1980
12. FLOWER MA, PARKER RP, COLES IP, et al: Feasibility of absolute activity measurements using the Cleon emission tomography system. *Radiology* 133:497-500, 1979
13. BUDINGER TF, GULLBERG GT, HUESMAN RH: Emission computed tomography. In *Image Reconstruction from Projections; Implementation and Applications.* Herman GT, Ed. Volume 32. *Topics in Applied Physics.* New York, Springer-Verlag, pp 147-246
14. HUESMAN RH: The effects of a finite number of projection angles and finite lateral sampling of projections on the propagation of statistical errors in transverse section reconstruction. *Phys Med Biol* 22:511-521, 1977
15. TER-POGOSSIAN MM: Basic principles of computed axial tomography. *Semin Nucl Med* 7:109-127, 1977